IOPscience iopscience.iop.org

Home Search Collections Journals About Contact us My IOPscience

An ultraviolet photodetector fabricated from WO_3 nanodiscs/reduced graphene oxide composite material

This content has been downloaded from IOPscience. Please scroll down to see the full text.

2013 Nanotechnology 24 295701

(http://iopscience.iop.org/0957-4484/24/29/295701)

View the table of contents for this issue, or go to the journal homepage for more

Download details:

IP Address: 128.113.26.88
This content was downloaded on 12/07/2016 at 22:28

Please note that terms and conditions apply.

Nanotechnology **24** (2013) 295701 (5pp) doi:10.1088/0957-4484/24/29/295701

An ultraviolet photodetector fabricated from WO_3 nanodiscs/reduced graphene oxide composite material

Dali Shao[1], Mingpeng Yu[2,3], Jie Lian[2] and Shayla Sawyer[1]

[1] Department of Electrical, Computer and Systems Engineering, Rensselaer Polytechnic Institute, Troy, NY 12180, USA
[2] Department of Mechanical, Aerospace and Nuclear Engineering, Rensselaer Polytechnic Institute, Troy, NY 12180, USA
[3] College of Materials Science and Engineering, Key Laboratory of Advanced Functional Materials, Ministry of Education, Beijing University of Technology, Beijing 100022, People's Republic of China

E-mail: shaod@rpi.edu

Received 12 January 2013, in final form 13 May 2013
Published 25 June 2013
Online at stacks.iop.org/Nano/24/295701

Abstract
A high sensitivity, fast ultraviolet (UV) photodetector was fabricated from WO_3 nanodiscs (NDs)/reduced graphene oxide (RGO) composite material. The WO_3 NDs/reduced GO composite material was synthesized using a facile three-step synthesis procedure. First, the Na_2WO_4/GO precursor was synthesized by homogeneous precipitation. Second, the Na_2WO_4/GO precursor was transformed into H_2WO_4/GO composites by acidification. Finally, the H_2WO_4/GO composites were reduced to WO_3 NDs/RGO via a hydrothermal reduction process. The UV photodetector showed a fast transient response and high responsivity, which are attributed to the improved carrier transport and collection efficiency through graphene. The excellent material properties of the WO_3 NDs/RGO composite demonstrated in this work may open up new possibilities for using WO_3 NDs/RGO for future optoelectronic applications.

(Some figures may appear in colour only in the online journal)

1. Introduction

UV photodetectors have been investigated for various commercial and military applications, such as in secure space-to-space communications, pollution monitoring, water sterilization, flame sensing and early missile plume detection [1]. To date, many different wide band gap semiconductors such as GaN, ZnO, Si_3N_4, and In_2O_3 nanostructures have been extensively studied for UV photodetector applications [2–5]. However, only a few studies reported using tungsten oxide (WO_3) nanomaterial for UV radiation detection [6, 7]. WO_3, as an n-type semiconductor material, has attracted considerable research interest due to its promising physical and chemical properties [8]. By virtue of its excellent electrochromic, optochromic, and gasochromic properties, WO_3 has great potential for gas sensor, environmental protection, and energy conversion applications [6–8]. WO_3 has potential for UV detection because of its indirect large energy band gap (3.3 eV) [7]. However, the UV photodetectors fabricated from WO_3 nanostructure showed very slow response times (>1 min) [6, 7]. Therefore, investigation of new WO_3 nanostructures for fast UV detection is highly desirable. Research on composite nanomaterial has attracted tremendous attention due to the possibility of multi-functional operation monolithically integrated on a single device [9, 10]. Graphene, as a novel carbon nanomaterial, has many remarkable material properties including high carrier transport mobility, large specific surface area, superior mechanical properties and excellent chemical stability [11–15]. However, large-scale production of graphene nanosheets remains a huge challenge and RGO has emerged as an inexpensive substitute for graphene [16]. The incorporation of RGO into the composites

 © 2013 IOP Publishing Ltd Printed in the UK & the USA

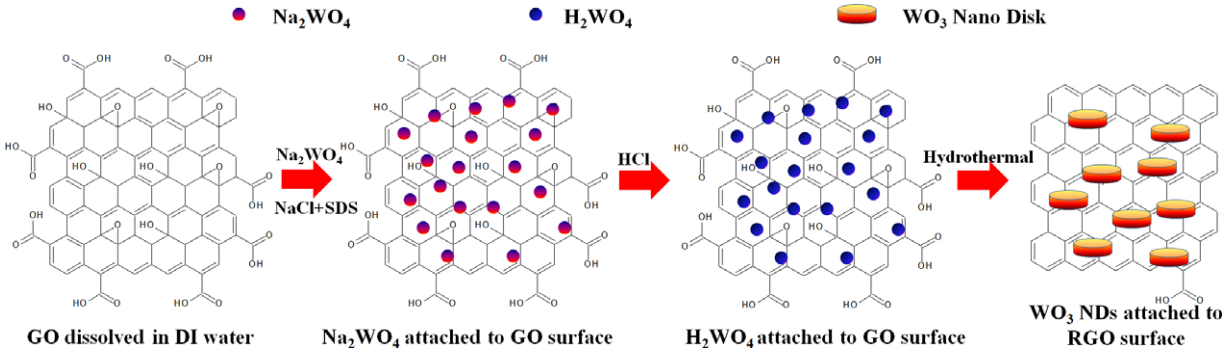

Figure 1. Scheme illustrating the growth mechanism of WO_3 NDs/RGO composite.

can provide them with the unique functions of RGO and also possibly induce intriguing properties inherited from the synergetic effect.

In this work, a facile three-step synthesis procedure was developed for the synthesis of novel WO_3 NDs/RGO composite material. First, the Na_2WO_4/GO precursor was synthesized by homogeneous precipitation. Second, the Na_2WO_4/GO precursor was transformed into H_2WO_4/GO composites by acidification. Finally, the H_2WO_4/GO composites were reduced to WO_3 NDs/RGO via hydrothermal reduction process. To demonstrate the optoelectronic properties of the WO_3 NDs/RGO composite material, a UV photodetector was fabricated by deposition of WO_3 NDs/RGO composite material on quartz substrate. Due to improved carrier transport and collection efficiency through RGO, the UV photodetector showed fast transient response and high photoresponsivity. The excellent optoelectronic properties of the WO_3 NDs/RGO composite may allow us to design various optoelectronic devices with high performance.

2. Experimental details

GO was prepared using a modified Hummers method [17]. GO powders were dispersed in deionized water to create a homogeneous dispersion (0.2 mg ml^{-1}) through ultrasonication for half an hour. WO_3 NDs/RGO composite material was grown through an *in situ* hydrothermal process. In a typical process, 1 g $Na_2WO_4{\cdot}2H_2O$, 0.2 g NaCl and 0.2 g SDS were dissolved in 40 ml GO solution and stirred for 6 h. Then, 2M hydrochloric acid solution was added dropwise to the above solution until the pH value of the solution was adjusted to approximately 2.0. After that, the solution was transferred into a Teflon-lined stainless steel autoclave (Parr, 4744) and heated to 180 °C. After 20 h of hydrothermal treatment, the autoclave was cooled down to room temperature naturally. The precipitate was centrifuged, washed with ethanol and deionized water six times, and finally dried at 60 °C under vacuum for further characterization. For comparison purposes, pure WO_3 NDs were also synthesized using a hydrothermal process without adding GO solutions.

The morphology and microstructure of the WO_3 NDs/RGO composite material was characterized by scanning electron microscopy (SEM, Carl Zeiss Ultra 1540). The crystal structure of the WO_3 NDs was confirmed using high resolution transmission electron microscopy (HRTEM, JEOL 2011). The x-ray diffraction (XRD, PANalytical) patterns of the WO_3 NDs/RGO composite material were measured at room temperature with Cu Kα radiation (wavelength = 1.54 Å). Raman spectroscopy was used to investigate the vibrational properties of the composite material. The chemical state of the composite material was characterized by x-ray photoelectron spectroscopy (XPS, PHI 5000 Versa Probe).

The UV photodetector was fabricated by deposition of WO_3 NDs/RGO composite on quartz substrate through the spin casting method. Then, interdigitated Al contacts with thickness of 300 nm were deposited on the top using an electron beam evaporator. A reference photodetector using WO_3 NDs was fabricated following the same procedure. The typical *I–V* characteristics of the photodetectors were measured using an HP4155B semiconductor parameter analyzer. The photoresponsivity spectra of the photodetectors were measured using a Shimadzu UV–visible 2550 spectrophotometer with a deuterium lamp (190–390 nm) and a halogen lamp (280–1100 nm).

3. Results and discussion

The scheme of the growth mechanism of WO_3 NDs/RGO composite material is shown in figure 1. First, due to the oxygen-containing functional groups on the GO sheets (hydroxyl, carbonyl, and epoxy groups), the GO surface can easily absorb Na^{2+} ions in aqueous solution through electrostatic interactions, and then interact with WO_4^{2-} to form Na_2WO_4 on GO sheets. Second, a large amount of H_2WO_4 was formed and attached to the surface of GO after the addition of HCl solution through an acidification process. Third, H_2WO_4 was decomposed into WO_3 crystal nuclei under a hydrothermal environment, which triggered the nucleation and preferential growth along *c*-axes in the presence of NaCl [17]. The hydroxyl, carbonyl, and epoxy groups located at the surface of the GO sheet act as anchor sites and enabled the subsequent formation of small WO_3 NDs on the surface. At the same time, hydrothermal reduction at high temperature was reported to be an effective route to restoring the sp^2-hybridized network. Thus, the increased temperature

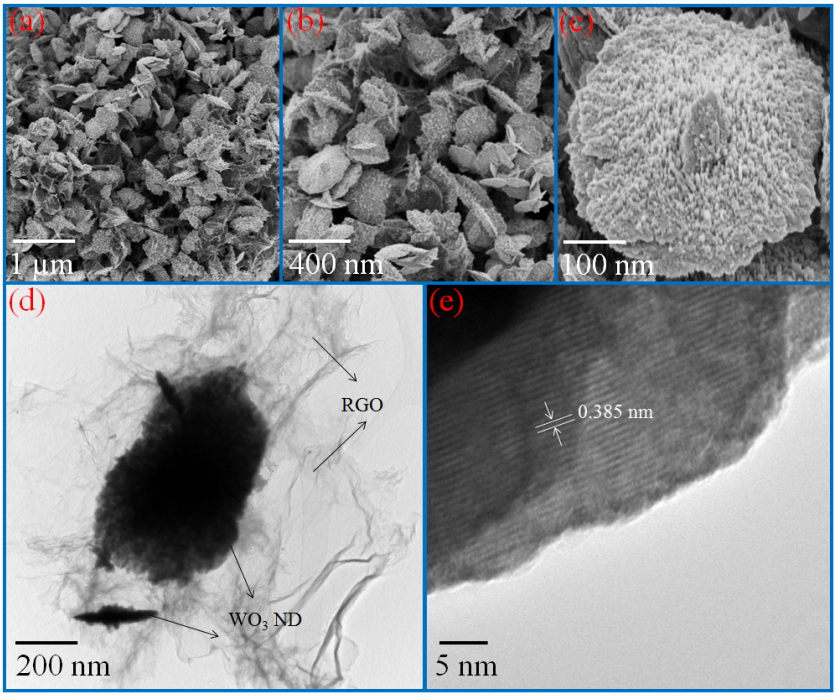

Figure 2. ((a)–(c)) High resolution SEM images of the WO_3 NDs/RGO composite material. (d) TEM and (e) HRTEM images of the WO_3 NDs/RGO composite material.

and pressure led to the rupture of oxygen-containing groups in the reaction. As a result, GO was simultaneously reduced to RGO, and this was accompanied with the growth of WO_3 NDs during the hydrothermal reaction.

The SEM images of the WO_3 NDs/RGO composite material are shown in figures 2(a)–(c). The average diameter and thickness of the WO_3 NDs are around 350 nm and 30 nm, respectively. A TEM image of the WO_3 NDs/RGO composite is shown in figure 2(d), from which both the WO_3 NDs and RGO can be well observed. Figure 2(e) shows an HRTEM image of the WO_3 NDs/RGO composite. The space of the lattice fringes is 0.385 nm, corresponding to the (001) plane of the WO_3 hexagonal cell. This confirms that the nanostructures are grown along the *c*-axis direction and is in agreement with JCPDS 33-1387. Figure 3(a) shows the x-ray diffraction (XRD) patterns of the WO_3 NDs/RGO composite material. All the peaks can be well indexed to the hexagonal structure of WO_3 (JCPDS 75-2187) with the space group $P6/mmm$. For the WO_3 NDs/RGO composite material, no obvious diffraction peaks of graphene are observed, which agrees well with a previous reported result [8]. The Raman spectrum of the composite material is shown in figure 3(b); the sharp peaks located at about ∼241 and ∼807 cm^{-1} are attributed to the O–W–O stretching mode [8]. Moreover, the band at ∼678 cm^{-1} was also reported for hexagonal WO_3 [18]. Two broad peaks centered at ∼1335 and ∼1595 cm^{-1} are assigned to the D and G bands of RGO, respectively. The D peak is attributed to the defects within the RGO while the G peak corresponds to the in-plane bond-stretching optical vibration of sp^2-hybridized carbon atoms. Figure 3(c) shows the W 4f core-level spectrum for the WO_3 ND/RGO composite material measured using XPS. Two major peaks for W $4f_{7/2}$ and W $4f_{5/2}$ were observed at 35.6 and 37.8 eV, respectively. These results are consistent with the previous report, indicating stoichiometric WO_3 in the composite [19].

The typical *I*–*V* characteristics of the photodetector fabricated from WO_3 NDs/RGO composite and the reference device were measured in the dark and with UV illumination at 335 nm with the intensity of 31.65 mW cm^{-2}, as shown in figure 4. The higher dark current of the WO_3 NDs/RGO composite device is attributed to improved conductivity of the composite through RGO. Note that the photocurrent of the WO_3 NDs/RGO composite device is almost 19 times higher than that of the reference device. Moreover, the photocurrent to dark current ratio of the WO_3 NDs/RGO composite device is around 50 at 20 V, which is ∼4 times higher than that of the reference device. These improvements are attributed to improved carrier transport and collection efficiency through RGO, which will be discussed in detail later. The initial low conductivity of the photodetectors in the dark environment is attributed to surface adsorbed oxygen molecules, which capture the free electrons from WO_3 NDs to form a negatively charged oxygen ion layer [$O_2(g) + e^- \rightarrow O_2{}^-(ad)$]. This process leads to the formation of a low conductivity depletion region near the surface. The depletion region created in the oxygen adsorption process can extend throughout the entire film due to the high surface to volume ratio of WO_3 NDs. Upon exposure to UV light, electron–hole pairs are generated in WO_3 NDs. The photogenerated holes can migrate to the surface of WO_3 NDs and recombine with the negative charged oxygen ions [$h^+ + O_2{}^-(ad) \rightarrow O_2(g)$], which results in a decrease in the width of the depletion region and an increase in the conductivity of the WO_3 NDs.

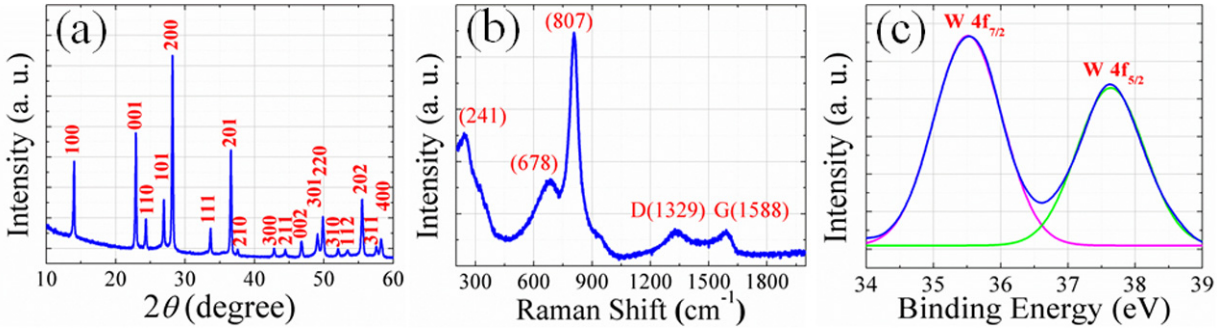

Figure 3. (a) XRD pattern and (b) Raman spectrum of the WO_3 NDs/RGO composite material. (c) W 4f peaks of the WO_3 NDs/RGO composite material.

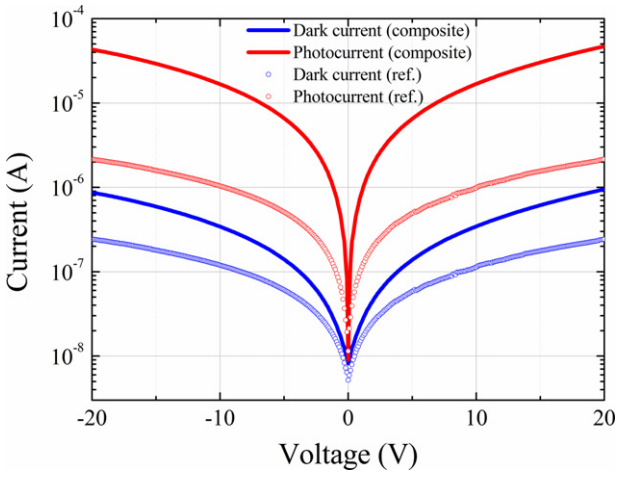

Figure 4. Typical *I*–*V* characteristics of the UV photodetectors fabricated from WO_3 NDs/RGO composite and from pure WO_3 NDs.

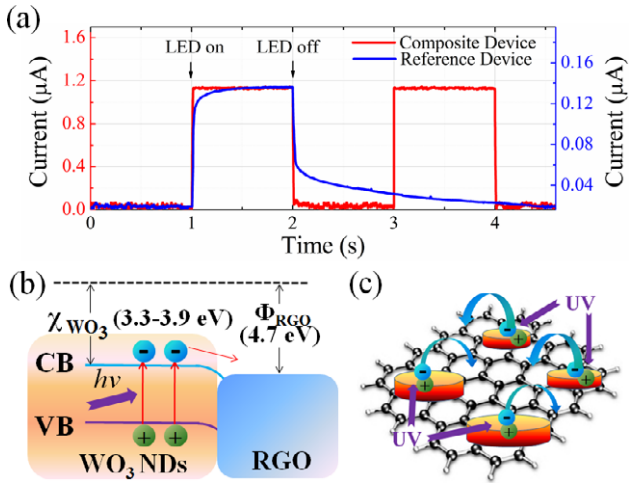

Figure 5. (a) Transient response of the UV photodetectors fabricated from WO_3 NDs/RGO composite and from pure WO_3 NDs. (b) Energy band alignment and (c) illustration of the carrier transport mechanism of the WO_3 NDs/RGO composite.

The transient responses of the WO_3 NDs/RGO composite photodetector and the reference device are shown in figure 5(a); they were measured by turning on and off a UV light emitting diode with peak wavelength at 335 nm. The rise time (as measured from 10% to 90%) and fall time (from 90% to 10%) of the WO_3 NDs/RGO composite photodetector were measured to be 13 and 16 ms, respectively. These are much faster than those of the reference device (rise time: ∼0.35 s, fall time: ∼2 s) and at least 100 times faster than for UV photodetectors fabricated from WO_3 nanowires [7].

The enhanced photocurrent and the fast transient response of the WO_3 NDs/RGO composite photodetector can be understood from the energy band diagram and the carrier transport process of the WO_3 NDs/RGO composite, as shown in figures 5(b) and (c), respectively. The electron affinity of the molecule WO_3 has been measured using different methods with a wide spread of values (3.33–3.94 eV) [20–23]. This is lower than the work function of the RGO, which is known to be around 4.7 eV below the vacuum level [24]. Thus, when WO_3 is in contact with the RGO, it is energetically favorable for the photogenerated electron to transfer from the conduction band of WO_3 to the RGO side. Since RGO has high carrier mobility, less accumulation of the electrons on the RGO side is expected. Therefore, the carrier transport efficiency can be effectively improved, leading to a fast rise of the photocurrent. When the UV illumination is turned off, the excess electrons in the RGO side transfer to the WO_3 side for recombination with holes, which is a very fast process. Thus fast decay was observed for WO_3 NDs/RGO composite material.

The photoresponsivity of the photodetectors, defined as photocurrent per unit of incident optical power, is shown in figure 6. A maximum photoresponsivity of 6.4 A W^{-1} at 347 nm was observed under 20 V bias for the WO_3 NDs/RGO composite, which is 17 times higher than that of the reference device and is more than 30 times higher than those of commercial GaN and SiC photodetectors (<0.2 A W^{-1}) [25]. To the best of our knowledge, this is the first report of photoresponsivity measured for WO_3 based UV photodetectors. The high responsivity of the WO_3 NDs/RGO composite is attributed to the internal gain introduced by the surface oxygen adsorption–desorption process, as well as improved carrier transport and collection efficiency obtained by employing the RGO.

4. Conclusion

In conclusion, a UV photodetector was fabricated from WO_3 NDs/RGO composite material synthesized using a facile three-step synthesis. A high photocurrent to dark current ratio

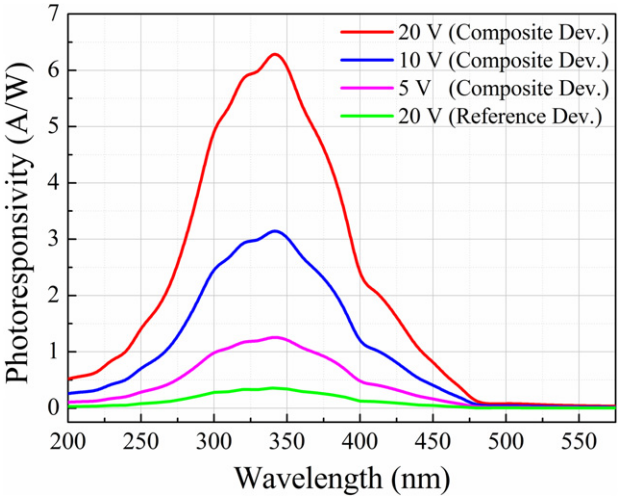

Figure 6. Photoresponsivity spectra of the UV photodetector fabricated from WO_3 NDs/RGO composite and from pure WO_3 NDs.

(600) is obtained under UV illumination at 340 nm for a bias of 20 V. The WO_3 NDs/RGO composite photodetector shows a fast transient response with a response time on the order of milliseconds. The improvement is attributed to improved carrier transport efficiency through RGO. A maximum photoresponsivity of 6.4 A W^{-1} at 347 nm was observed under 20 V bias. These results will open up new possibilities for using WO_3 NDs/RGO for future optoelectronic applications such as in high-performance ultraviolet radiation sensing, optical keys and optical memory. Further exploration in this direction is highly desirable.

Acknowledgments

The authors gratefully acknowledge support from National Security Technologies through NSF Industry/University Cooperative Research Center Connection One. The authors also acknowledge the National Science Foundation Smart Lighting Engineering Research Center (EEC-0812056) and an NSF career award DMR 1151028. The author Yu thanks the China Scholarship Council (CSC File No. 2010646040) for financial support.

References

[1] Blank T V and Gol'dberg Y A 2003 Semiconductor photoelectric converters for the ultraviolet region of the spectrum *Semiconductors* **37** 999–1030
[2] Li D, Sun X, Song H, Li Z, Chen Y, Jiang H and Miao G 2012 Realization of a high-performance GaN UV detector by nanoplasmonic enhancement *Adv. Mater.* **24** 845–9
[3] Soci C, Zhang A, Xiang B, Dayeh S A, Aplin D P R, Park J, Bao X Y, Lo Y H and Wang D 2007 ZnO nanowire UV photodetectors with high internal gain *Nano Lett.* **7** 1003–7
[4] Zhang J Y, Chen Y X, Guo T L, Lin Z X and Wang T H 2007 Sub-band-gap photoconductivity of individual α-Si_3N_4 nanowires *Nanotechnology* **18** 325603
[5] Shao D, Qin L and Sawyer S 2012 High responsivity, bandpass near-UV photodetector fabricated from PVA–In_2O_3 nanoparticles on a GaN substrate *IEEE Photon. J.* **4** 715–20
[6] Huang K, Zhang Q, Yang F and He D 2010 Ultraviolet photoconductance of a single hexagonal WO_3 Nanowire *Nano Res.* **3** 281–7
[7] Li L, Zhang Y, Fang X, Zhai T, Liao M, Sun X, Koide Y, Bando Y and Golberg D J 2011 WO_3 nanowires on carbon papers: electronic transport, improved ultraviolet-light photodetectors and excellent field emitters *Mater. Chem.* **21** 6525–30
[8] An X, Yu J C, Wang Y, Hu Y, Yu X and Zhang G 2012 WO_3 nanorods/graphene nanocomposites for high-efficiency visible-light-driven photocatalysis and NO_2 gas sensing *J. Mater. Chem.* **22** 8525–31
[9] Liu J, Jiang J, Cheng C, Li H, Zhang J, Gong H and Fan H J 2011 Co_3O_4 nanowire@MnO_2 ultrathin nanosheet core/shell arrays: a new class of high-performance pseudocapacitive materials *Adv. Mater.* **23** 2076–81
[10] Zhou W *et al* 2011 Epitaxial growth of branched α-Fe_2O_3/SnO_2 nanoheterostructure with improved lithium-ion battery performance *Adv. Funct. Mater.* **21** 2439–46
[11] Watcharotone S *et al* 2007 Graphene–silica composite thin films as transparent conductors *Nano Lett.* **7** 1888–92
[12] Ponomarenko L A, Schedin F, Katsnelson M I, Yang R, Hill E W, Novoselov K S and Geim A K 2008 Chaotic Dirac billiard in graphene quantum dots *Science* **320** 356–8
[13] Wang X, Zhi L and Mullen K 2008 Transparent, conductive graphene electrodes for dye-sensitized solar cells *Nano Lett.* **8** 323–7
[14] Girit C O *et al* 2009 Graphene at the edge: stability and dynamics *Science* **323** 1705–8
[15] Geim A K and Novoselov K S 2007 The rise of graphene *Nature Mater.* **6** 183–91
[16] Shen J, Yan B, Shi M, Ma H, Li N and Ye M 2011 One step hydrothermal synthesis of TiO_2-reduced graphene oxide sheets *J. Mater. Chem.* **21** 3415–21
[17] Wang G, Sun X, Lu F, Sun H, Yu M, Jiang W, Liu C and Lian J 2012 Flexible pillared graphene–paper electrodes for high-performance electrochemical supercapacitors *Small* **8** 452–9
[18] Ha J-H, Muralidharan P and Kim D K 2009 Hydrothermal synthesis and characterization of self-assembled h-WO_3 nanowires/nanorods using EDTA salts *J. Alloys Compounds* **475** 446–51
[19] Bueno P R, Pontes F M, Leite E R, Bulhões L O S, Pizani P S, Lisboa-Filho P N and Schreiner W H 2004 Structural analysis of pure and $LiCF_3SO_3$-doped amorphous WO_3 electrochromic films and discussion on coloration kinetics *J. Appl. Phys.* **96** 2102–9
[20] Jensen D E and Miller W J 1970 Electron attachment and compound formation in flames. III. Negative ion and compound formation in flames containing tungsten and potassium *J. Chem. Phys.* **53** 3287–92
[21] Center R E 1972 Ion—molecule experiments involving negative ions of tungsten and rhenium oxides *J. Chem. Phys.* **56** 371–6
[22] Rudnyi E B, Sidorov L N, Vovk O M and Kaibicheva E A 1989 Formation enthalpies of oxygen-containing anions of group-VI elements in the gas-phase and the electron affinities of CrO_3, MoO_3, and WO_3 *J. Chem. Thermodyn.* **21** 247–58
[23] Walter C W, Hertzler C F, Devynck P, Smith G P and Peterson J R J 1991 Photodetachment of WO_3^-: the electron affinity of WO_3 *Chem. Phys.* **95** 824–7
[24] Kong B S, Geng J and Jung H T 2009 Layer-by-layer assembly of graphene and gold nanoparticles by vacuum filtration and spontaneous reduction of gold ions *Chem. Commun.* **16** 2174–6
[25] Jin Y Z, Wang J P, Sun B Q, Blakesley J C and Greenham N C 2008 Solution-processed ultraviolet photodetectors based on colloidal ZnO nanoparticles *Nano Lett.* **8** 1649–53